Journal Pre-proofs

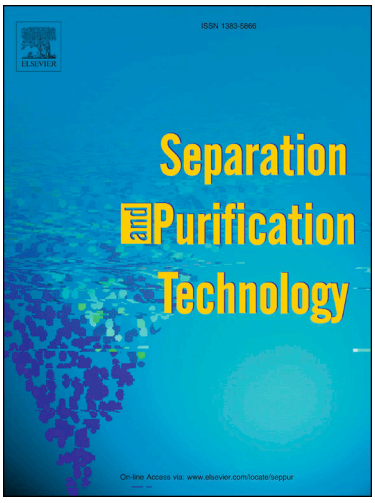

Recovery and concentration of ammonia from return liquor to promote enhanced CO_2 absorption and simultaneous ammonium bicarbonate crystallisation during biogas upgrading in a hollow fibre membrane contactor

S. Bavarella Conceptualisation, M. Hermassi, A. Brookes, A. Moore, P. Vale, I.S. Moon, M. Pidou, E.J. McAdam

PII: S1383-5866(19)34535-6
DOI: https://doi.org/10.1016/j.seppur.2020.116631
Reference: SEPPUR 116631

To appear in: *Separation and Purification Technology*

Received Date: 3 October 2019
Revised Date: 22 January 2020
Accepted Date: 26 January 2020

Please cite this article as: S. Bavarella Conceptualisation, M. Hermassi, A. Brookes, A. Moore, P. Vale, I.S. Moon, M. Pidou, E.J. McAdam, Recovery and concentration of ammonia from return liquor to promote enhanced CO_2 absorption and simultaneous ammonium bicarbonate crystallisation during biogas upgrading in a hollow fibre membrane contactor, *Separation and Purification Technology* (2020), doi: https://doi.org/10.1016/j.seppur.2020.116631

Separation and Purification Technology, Volume 241, June 2020, Article number 116631
DOI: 10.1016/j.seppur.2020.116631

Recovery and concentration of ammonia from return liquor to promote enhanced CO_2 absorption and simultaneous ammonium bicarbonate crystallisation during biogas upgrading in a hollow fibre membrane contactor

S. Bavarella[a], M. Hermassi[a], A. Brookes[b], A. Moore[c], P. Vale[d], I.S. Moon[e], M. Pidou[a], E.J. McAdam[a,*]

[a]Cranfield Water Science Institute, Vincent Building, Cranfield University, Bedfordshire, MK43 0AL, UK
[b]Anglian Water, Block C-Western House, Peterborough Business Park, Lynch Wood, Peterborough PE2 6FZ, UK
[c]Northumbrian Water, Boldon House, Wheatlands Way, Durham DH1 5FA, UK
[d]Severn Trent Water, 2 St. Johns Street, Coventry CV1 2LZ, UK
[e]Department of Chemical Engineering, Sunchon National University, Suncheon-si, 57922, Rep. of Korea
*Corresponding Author: e.mcadam@cranfield.ac.uk

Abstract

In this study, thermal desorption was developed to separate and concentrate ammonia from return liquor, for use as a chemical absorbent in biogas upgrading, providing process intensification and the production of crystalline ammonium bicarbonate as the final reaction product. Applying modest temperature (50°C) in thermal desorption suppressed water vapour pressure and increased selective transport for ammonia from return liquor ($0.11M_{NH3}$) yielding a concentrated condensate (up to $1.7M_{NH3}$). Rectification was modelled through second-stage thermal processing, where higher initial ammonia concentration from the first stage increased mass transfer and delivered a saturated ammonia solution ($6.4M_{NH3}$), which was sufficient to provide chemically enhanced CO_2 separation and the simultaneous initiation of ammonium bicarbonate crystallisation, in a hollow fibre membrane contactor. Condensate recovered from return liquor exhibited a reduction in surface tension. We propose this is due to the stratification of surface active agents at the air-liquid interface during primary-stage thermal desorption which carried over into the condensate, 'salting' out CO_2 and lowering the kinetic trajectory of absorption. However, crystal induction (the onset of nucleation) was comparable in both synthetic and thermally recovered condensates, indicating the thermodynamics of crystallisation to be unaffected by the recovered condensate. The membrane was evidenced to promote heterogeneous primary nucleation, and the reduction in the recovered condensate surface tension was shown to exacerbate nucleation rate, due to the reduction in activation energy. X-ray diffraction of the crystals formed, showed the product to be ammonium bicarbonate, demonstrating that thermal desorption eliminates cation competition (e.g. Ca^{2+}) to guarantee the formation of the preferred crystalline reaction product. This study identifies an important synergy between thermal desorption and membrane contactor technology that delivers biogas upgrading, ammonia removal from wastewater and resource recovery in a complimentary process.

Keywords: *membrane contactor; biogas; ammonia return liquor; precipitation; thermal stripping; crystallisation*

1. Introduction

By removing carbon dioxide (CO_2) from biogas, the 'upgraded' biomethane offers new value as vehicle fuel or as natural gas substitute (Persson et al., 2007). A large number of biogas upgrading plants are now installed in Europe. Packed column absorbers are typically used with water or chemical solvents. The costs involved are significant and chemical solvents can be used to reduce cost through process intensification. Whilst chemical absorption is a mature technology in the water sector for odour management (Esquiroz-Molina et al., 2013), different chemical solvents are required for CO_2 separation. In carbon capture and storage (CCS), ammonia (NH_3) has been investigated due to its greater absorption capacity, lower energy requirement for regeneration and lower purchase price. However, its higher vapour pressure results in NH_3 slip (Kozak et al., 2009).

Hollow fibre membrane contactors (HFMC) are an alternative to packed columns and introduce a hydrophobic microporous membrane between the gas and liquid phases. This facilitates non-dispersive contact, where only gases can pass through the pores (Heile et al., 2014; Vecino et al., 2019). McLeod et al. (2014) showed that NH_3 slip could be minimised in HFMC due to the laminar conditions imposed, promoting radial diffusion of NH_3 from the absorbent bulk to the boundary layer, which also stabilised NH_3 to non-volatile ammonium (NH_4^+) through the overall counter-current chemical reaction (CO_2/NH_3) (Budzianowski, 2011a):

$$CO_2 + NH_3 + H_2O \rightarrow NH_4HCO_3(\text{s}) \quad (1)$$

Whilst the membrane introduces an additional resistance to mass transfer, the increased specific surface area in HFMCs provides substantive process intensification when compared to packed columns, and when complemented by chemical reaction, can provide significantly lower capital and operational costs versus conventional biomethane solutions (Belaissaoui and Favre, 2018).

Biogas upgrading facilities are co-located to ammonia rich wastewaters which could provide a sustainable source of absorption solvent for biogas upgrading. McLeod et al. (2014)

illustrated a 15 times enhancement in CO_2 mass transfer with NH_3 rich sludge liquor returns (2000 mgNH_4^+-N L^{-1}, 0.11 mol L^{-1}). He et al. (2017) instead pre-concentrated NH_3 from return liquors to 18,300 mgNH_4^+-N L^{-1} (1.3 mol L^{-1}) using vacuum membrane distillation (VMD) to increase solution reactivity during biogas upgrading. This remains below the ammonia concentration generally considered viable for CCS (>2.5 mol L^{-1}) due to the thermal requirements in absorbent regeneration (Mani et al., 2006; Budzianowski, 2011b). However, the authors cleverly proposed discharge of the used absorbent for fertigation (Bonet-Ruiz et al., 2015), thereby removing the need for solvent thermal regeneration and simplifying operation.

Alternatively, by transforming the NH_3-CO_2 reaction product into crystalline ammonium bicarbonate (NH_4HCO_3), the cost for biological treatment of side-stream ammonia (return liquors) is circumvented (~€1.9 to 83.3 per kgNH_4^+-N; Oxera, 2006), and the tankering requirement versus a fertigation approach can be avoided. Fixation of CO_2 into NH_4HCO_3 (flux around 2000 kg h^{-1}) produces an industrially important crystalline feedstock (e.g. manufacture of plastics, ceramics, inks) with a wholesale cost of € 0.11 kg^{-1} (Veiga et al., 1999; Mortson and Telesz, 2001; Budzianowski, 2011b). Ammonium bicarbonate crystallisation was first considered in CCS to reduce the heat requirement for regeneration (Darde et al., 2009). However, the homogeneous nucleation and growth of crystals within the mixed phase of a packed column introduced clogging of equipment, making implementation difficult (Sutter et al., 2015). McLeod et al. (2015) successfully demonstrated the feasibility of ammonium bicarbonate crystallisation in a HFMC using a synthetic ammonia solution. The high contact angle exhibited by the hydrophobic membrane, lowered the activation energy sufficiently to promote heterogeneous nucleation at the micropore where interaction of the gas, liquid and membrane was mediated, inducing surface growth of the reaction product. A combination of controlled nucleation and phase separation fostered by the membrane, enabled recovery of the reaction product downstream in the liquid phase (McLeod et al., 2015). Membrane contactors therefore offer the unique opportunity to simultaneously accomplish enhanced CO_2 separation to reduce biomethane production costs, introduce side-stream NH_3 removal from

return liquors to reduce the cost of treatment (Ma et al., 2019), and enable the crystallisation of ammonium bicarbonate which offer a new value stream, all within a single processing stage.

Previous studies on ammonia crystallisation within real solutions have reported the final reactant concentration to be below the solubility limit, such that crystallisation could not proceed. For example, Ukwuani and Tao (2016) coupled ammonia stripping with second stage acid absorption to recover crystalline ammonium sulphate. However, an antisolvent or distillation step was needed to overcome the high solubility limit (706 g L^{-1}), thus requiring a third crystallisation stage. Similarly, when return liquor was used for CO_2 absorption, distillation was required to initiate crystallisation due to the solubility limit for NH_4HCO_3 (182 g L^{-1} or 2.3 mol_{NH3} L^{-1} at 20°C) (McLeod et al., 2014). This was further complicated by the presence of competing cations which produced more thermodynamically favourable crystals (e.g. calcium carbonate, sodium bicarbonate) over ammonium bicarbonate. Teichgräber and Stein (1994) proposed that thermal stripping of return liquor in a packed column could achieve an ammonia concentration of 130 gNH_4^+ L^{-1} (7.2 mol_{NH3} L^{-1}) which is sufficient for crystallisation. Whilst only theorised, we suggest thermally concentrating ammonia from return liquor will provide a reactive solution sufficient to permit NH_4HCO_3 crystallisation directly after reaction such that CO_2 separation and product conversion occur in a single stage membrane process. Since thermal stripping is selective for NH_3 (based on volatility), it is also asserted that competing cations will be limited, favouring the formation of crystalline ammonium bicarbonate.

In this study, we therefore seek to demonstrate an integrated system comprising thermal stripper and membrane contactor for chemically enhanced CO_2 separation with pre-concentrated ammonia recovered from real wastewater, to improve the value proposition from biomethane production by coupling NH_4HCO_3 crystallisation within the a single stage HFMC. The objectives were to: (i) determine the boundary conditions needed to super-concentrate ammonia from return liquor; (ii) apply these conditions to demonstrate ammonia separation and recovery from real wastewater using thermal stripping; (iii) compare CO_2 absorption and crystallisation behaviour using synthetic and recovered ammonia solutions of equal reactivity;

and (iv) confirm the crystalline reaction product derived from real wastewater to be NH_4HCO_3 to evidence the reduction in cationic competition through application of pre-treatment.

2. Material and methods

2.1 Experimental set-up for thermal stripping of ammonia

Thermal stripping was conducted using a rotary evaporator (Rotavapor R-100, Buchi Ltd, Oldham, UK) (Figure 1A). The feed volume (1L) was brought to temperature and a vacuum applied. Each set of operating conditions (vacuum, pH, temperature) were conducted in triplicate. The volume, pH, conductivity (Jenway 4330, Cole-Parmer, Stone, UK), temperature (-50 to 150°C, Cole Parmer, St. Neots, UK) and NH_3 concentration of residual feed and condensate were determined to permit mass balance and process kinetics to be established (Ukwuani and Tao, 2016). Equilibrium between ammonium and ammonia is strongly dependent upon pH and temperature (Figure A1) (Bates and Pinching, 1949; Perry and Green, 2007):

$$\alpha_{NH_3} = 1/(1 + 10^{pK_a^S - pH}) \quad (2)$$

$$pK_{a,T}^S = pK_{a,298}^S + 0.0324(298 - T) \quad (3)$$

$$pK_{a,P}^S = pK_{a,1}^S + 0.0415P/T \quad (4)$$

Where α_{NH3} is the relative fraction of free ammonia; pK_a^S is the negative logarithm of stoichiometric acid hydrolysis constant of ammonium ion; $pK_{a,T}^S$ and $pK_{a,P}^S$ are the pK_a^S values at temperature T and 298K respectively. During stripping, ammonia volatilisation is driven by the difference between the saturation concentration and solution concentration, as expressed by Lewis-Whitman model (Tao and Ukwuani, 2015):

$$J_{NH_3\,stripped} = -K_L \frac{A}{V}(C - C_s) \quad (5)$$

where $J_{NH3\ stripped}$ is rate of ammonia mass transfer (mg L^{-1} h^{-1}), K_L is overall liquid-phase mass transfer coefficient (m h^{-1}), C_s is NH_3 saturation concentration (mg L^{-1}), C is NH_3 solution concentration at time t (mg L^{-1}) and A/V is area-volume ratio of the liquid (36.2 m^2 m^{-3}). Ammonia saturation concentration decreases with temperature (Figure A2) (O'Neil, 2013),

while its variation with vacuum pressure in the range 10 to 101.3 kPa is negligible (Whitfield, 1974; Salavera et al., 2005). By integrating (5) from t=0 to t=t+1:

$$\ln\left(\frac{C - C_s}{C_0 - C_S}\right) = -K_L\frac{A}{V}t \quad (6)$$

The water flux (J_{H2O}, g h^{-1}) can be expressed as (He et al., 2018):

$$J_{H2O\ recovered} = \frac{\Delta m_{H2O}}{\Delta t} \quad (7)$$

where Δm_{H2O} (g) is the mass of water transferred from the feed to the condensate. Ammonia loss ($J_{NH3\ loss}$, mg L^{-1} h^{-1}) and ammonia recovered ($J_{NH3\ recovered}$, mg L^{-1} h^{-1}) were determined by:

$$J_{NH3\ loss} = \frac{C_0V_0 - C_tV_t - C_{rec,\ t}V_{rec,\ t}}{\Delta t} \quad (8)$$

$$J_{NH3\ recovered} = J_{NH3\ stripped} - J_{NH3\ loss} \quad (9)$$

where V_0, V_t, feed volume at time t=0 and time t=t+1, while $V_{rec,t}$ and $C_{rec,t}$ are volume (L) and ammonia concentration (mg L^{-1}) in the recovered condensate at time t=t+1.

2.2 Membrane contactor experimental set-up

A single micro-porous polypropylene hollow fibre (Membrana GmbH, Wuppertal, Germany), comprised of 0.2 µm nominal pore size and active fibre length of 165 mm (Table A1) was fitted in a Perspex cell comprising a 12 mm diameter channel (Figure 1b). The fibre was potted using epoxy resin (Bostick Ltd., Stafford, UK). Carbon dioxide (99.8%, BOC gases, Ipswich, UK) was fed into the lumen of the hollow-fibre at 1000 mL min^{-1} or 1.7 x 10^{-5} m^3 s^{-1} (19±1°C) using a laminar mass flow controller (0.01-1 L min^{-1}, Roxspur Measurement and Control Ltd., Sheffield, UK), while the absorbent was recirculated counter-currently on the shell-side of the hollow-fibre at 200 mL min^{-1} or 3.3 x 10^{-6} m^3 s^{-1} (Watson-Marlow 520Du, Watson-Marlow Ltd., Falmouth, UK). Absorbent temperature was sustained at 6±1°C using a chiller (R1, Grant Instruments Ltd., Cambridge, UK). Thermocouples (K-type, Thermosense Ltd., Bucks, UK) were positioned in the gas and liquid upstream and downstream of the cell to determine temperature in real time.

2.3 Reagents and analytical methods

Synthetic ammonia containing wastewater were prepared by diluting NH_4OH (35%, 2.5 L, Fisher Chemicals) into de-ionised water. Ammonia concentration was determined using proprietary pre-prepared cell test (4-80 mg L^{-1}, VWR International Ltd., Poole, UK) followed by quantitation using spectrophotometry. Solution pH was fixed using hydrochloric acid (37%, Fisher Scientific, Loughborough, UK). For crystallisation experiments, feed concentration was fixed to pH 10, which is typically used in CO_2-NH_3 absorption (Yeh et al., 2005) and ammonia concentration fixed at 3.3 mol_{NH3} L^{-1} as this concentration has been shown to limit wetting (Bavarella, 2018). For real wastewater experiments, return liquor was collected from a local wastewater treatment works (Table 1).

A bubble flow meter (1000 mL, SKC, Blandford Forum, UK) was used to determine carbon dioxide flux (J_{CO2}, mol m^{-2} s^{-1}):

$$J_{CO_2} = \frac{(Q_{G,in} - Q_{G,out}) \times 273.15 \times 1000}{22.4 \times A_m T_G} \quad (10)$$

where $Q_{G,in}$ and $Q_{G,out}$ are gas flow rate (m^3 s^{-1}) before and after HFMC, A_m is the membrane surface area for absorption (m^2) and T_G is the gas temperature (K) (Atchariyawut et al., 2007). Bicarbonate concentration was measured using UV absorption at 215nm (Wilson et al., 2001; Mookherji et al., 1966; Birkmann et al., 2018) (Jenway 6715, Cole-Parmer, Stone, UK). Solvent surface tension was determined using a Du Noüy ring tensiometer (Kruss K6, Bristol, UK). Each experimental trial was terminated at a fixed level of supersaturation (C/C*), defined as the ratio between the CO_2 absorbed and the CO_2 required to form ammonium bicarbonate at the solubility limit. Experimental trials at each supersaturation level were conducted in triplicate. Whilst experiments with the condensate recovered from real wastewater were also conducted in triplicate, due to the limited volume of the recovered fraction, only one supersaturation level could be characterised. Following crystallisation, the absorbent was filtered through a 0.45 μm filter (Whatman, Camlab Ltd., Cambridge, UK) and weighed. Crystals were immersed in anhydrous alcohol to minimise agglomeration during counting (Veiga et al., 1999) and deposited onto a microscope slide consisting of a 1 mm grid. The slide

was placed under an optical microscope (Optech Microscope Services Ltd., Thame, UK), equipped with PL 5/0.12 lens and digital camera (Infinity 3, Lumenera, Ottawa, Canada). Images were analysed with image processing software (Image Pro Plus, Media Cybernetics, Cambridge, UK) to determine crystal number and size. Each image analysed corresponded to around 50 crystals. For each sacrificial test, at least 600 crystals were classified to develop a statistically representative crystal size distribution (CSD) which was constructed using a log-normal distribution (Ji et al., 2010). The recovered crystals were exposed to x-ray diffraction with Cu Ka1 radiation (Siemens D5005 X-ray diffractometer, Bruker UK Ltd., Coventry, UK) using 0.04° steps and diffraction patterns recorded in the 2θ range 15-40° (Meng et al., 2005).

3. Results

3.1 Identifying boundary conditions for thermal stripping of ammonia from wastewater

The impact of temperature was investigated at solution pH 11 to ensure that the equilibrium was shifted toward ammonia (Figure A1). For this low concentration solution (0.11 mol_{NH3} L^{-1}), ammonia mass transfer increased sharply with temperature, from K_L 0.09 mm h^{-1} or 2.5 x 10^{-8} m s^{-1} at 50°C to 2.6 mm h^{-1} or 7.2 x 10^{-7} m s^{-1} at 80°C (Figure 2). However, the highest ammonia concentration was identified in the condensate (the recovered fraction) at the lowest temperature (Figure 3). To illustrate, at an equivalent condensate volume (2.3%, $V_{recovered}/V_{initial\ feed}$), the condensate at 50°C and 80°C was 1.3 mol_{NH3} L^{-1} and 0.2 mol_{NH3} L^{-1} respectively from an initial feed solution concentration of 0.11 mol_{NH3} L^{-1}. An increase in solution pH up to 10 increased condensate ammonia concentration, after which a similar ammonia concentration of around 2 mol_{NH3} L^{-1} was realised (Figure 4). At pH = 10, the equilibrium at 80°C is shifted toward 100% free ammonia (Figure A1). A range of higher initial ammonia concentrations were examined to represent the impact of in-series thermal stripping (rectification) (Figure 5). A positive linear relationship was identified between initial feed ammonia concentration and the liquid phase ammonia mass transfer coefficient which increased from 1.2 to 14.1 mm h^{-1} (or 3.3 x 10^{-7} to 3.9 x 10^{-6} m s^{-1}) for feed ammonia concentrations of 0.5 and 2.7 mol_{NH3} L^{-1}, respectively. The mass transfer coefficient recorded for 0.5 mol_{NH3} L^{-1} was below that recorded

for the natural wastewater concentration (0.11 mol_{NH3} L^{-1}; Figure 2) which can be accounted for by the higher volumetric conversion (longer run-time) and lower vacuum pressure. Whilst the higher K_L increased the volumetric conversion into condensate over the fixed time period, a similar condensate ammonia concentration of around 6 mol_{NH3} L^{-1} was identified for each initial feed concentration trialled, and approximated to the solubility limit of ammonia in water at 80°C (Figure A2).

3.2 Characterisation of condensate recovered from real return liquor

The real return liquor ammonia concentration was 2,380 $mgNH_4^+$ L^{-1} (0.14 mol_{NH4+} L^{-1}). The COD and total suspended solids concentrations were 6,100 and 6,600 mg L^{-1} respectively (Table 1). The return liquor pH was increased to 11, and subjected to a two-stage thermal desorption to mimic the rectification process that would be employed at larger scale (Table 2). In the first stage, ammonia concentration in the recovered condensate was increased to 47,600 $mgNH_3$ L^{-1} (2.8 mol_{NH3} L^{-1}), which increased further to 108,000 $mgNH_3$ L^{-1} (6.4 mol_{NH3} L^{-1}) following the second stage thermal desorption. The recovered condensate was low in total suspended solids (<5 mg L^{-1}), equivalent to a particulate COD removal of 94.5%, but did comprise of a soluble chemical oxygen demand (sCOD) concentration of 1678 mg L^{-1} (Figure A3). The difference in solution surface tension was evaluated, as this presents implications for membrane wetting (which will reduce CO_2 mass transfer) and the induction of crystallisation. The difference in surface tension of the synthetic ammonia solution and the thermally recovered condensate (return liquor) from that of water (σ 72.8 mN m^{-1}) were around Δσ +0.9 and -39 mN m^{-1} respectively at an ammonia concentration of 3.3 mol_{NH3} L^{-1} (Figure 6).

3.3 CO_2 absorption and NH_4HCO_3 crystallisation in real and synthetic wastewater

Ammonia concentration of synthetic and real solutions were fixed to 3.3 mol_{NH3} L^{-1} for absorption experiments (Table 1). Initial CO_2 fluxes were similar for the synthetic and the condensate recovered from return liquor, but following progressive absorption of CO_2, a more notable decline in CO_2 flux was observed for the condensate recovered from return liquor

(Figure 7). Whilst absorption kinetics were slower for the real solution, the reduction in pH induced by the formation of ammonium carbamate following the continued inclusion of CO_2 (McLeod et al., 2015) were comparable at an equivalent amount of CO_2 absorbed (based on mass balance of the gas phase) (Figure 8). As CO_2 absorption progressively decreased solution pH further, an increase in bicarbonate concentration (measured using absorption at UV_{215nm} as a surrogate indicator) was noted which peaked around a supersaturation level (C/C*) of 1 for both solutions (Figure 7). Whilst comparable bicarbonate trends were similarly evidenced for both solutions, lower UV_{215nm} absorbance was identified for the real solution which can be accounted for by the comparatively higher turbidity of the sample (particulate chemical oxygen demand, pCOD, 89 mg L^{-1}) subsequently limiting solution absorbance; analogous bicarbonate transformation was thus confirmed through observation of the initiation of crystallisation at the same supersaturation level (C/C*, 1.7). Very few, if any, crystals resided on the membrane, and were instead primarily recovered in the bulk solution downstream of the membrane (Figure 9); this was supported by mass balance which demonstrated that over 90% of the nitrogen removed from solution, was resident within the crystalline phase recovered downstream. Upon increasing levels of supersaturation, an increase in crystal number (expressed as number per cubic centimetre, N cm^{-3}) and crystal size was observed for the downstream crystal population within the synthetic solution reaching 5 N cm^{-3} and 424 µm respectively at C/C* 2.1 (Figure 10). For comparison, crystal number and crystal size of 75 N cm^{-3} and 601 µm were respectively recorded for the downstream crystal population within the recovered condensate at an equivalent level of supersaturation. To examine crystallinity of the recovered crystals, crystals produced within the bulk solution of the synthetic solution and the condensate recovered from return liquor were exposed to X-ray diffraction, and compared to the analysis of pure ammonium bicarbonate (>99%) as a reference (Figure 11). Each of the major 2θ reference peaks were identified within the crystals formed from synthetic and real solutions, indicating that the crystal phase is primarily ammonium bicarbonate (Meng et al., 2005). Most minor 2θ reference peaks also correlated to the reference material, with some small mismatch in position, which can be accepted as

experimental error (e.g. specimen displacement). Whilst peak position correlates to the chemical composition, physical and chemical properties, the 2θ peak intensity can also be influenced by the crystal habit since the total area of each face is different (Inoue and Hirasawa, 2013). Such shifts in habit from those observed in the reference material, were experimentally observed in this study (Figure 9).

4. Discussion

In this study, the use of ammonia rich condensate, recovered through thermal stripping of return liquor, was demonstrated to facilitate CO_2 separation and initiate the controlled growth and recovery of crystalline ammonium bicarbonate in a chemically reactive membrane crystallisation reactor, based on hollow fibre membrane contactor technology. Thermal stripping at elevated temperature (80°C) raised the saturated vapour pressure of NH_3 (Figure A2; Wilson, 1925) and guaranteed a shift in the ammonia-ammonium equilibrium toward ammonia. This increased the overall mass transfer coefficient (Figure 2) and is comparable to observations by Tao and Ukwuani (2015). This transition in the pKa with an increase in temperature is important, as it evidences through optimisation that it may be possible to shift the ammonia-ammonium equilibrium toward ammonia with only limited chemical demand. For example, at 70°C, over 90% of the nitrogen is present as ammonia (Figure A1), which requires pH correction of the return liquor by only 0.5 pH unit, the mediation of such a change having been demonstrated through using stripping technology as an alternative to direct chemical addition (Kinidia et al., *In Press*). However, lowering stripper temperature (50°C) increased the recovered condensate ammonia concentration by suppressing the relative vapour pressure for water, which induced selectivity toward ammonia (Thurston et al., 1979; O'Neil, 2013). In second-stage thermal stripping, the highest rate of mass transfer was recorded by increasing initial ammonia concentration. Therefore, when applying rectification at industrial scale for ammonia recovery, which is analogous to distillation columns in series being consolidated within a single stage process, operation at lower ΔT may be more pragmatic as this limits energy demand, and delivers a higher ammonia concentration which will

subsequently enhance mass transfer in the overall separation (Teichgräber and Stein, 1994). Improvement in the overall rate of mass transfer during thermal desorption can also be realised through and increase in the specific interfacial surface area (over an order of magnitude) and hydrodynamic optimisation that would be expected upon the transition from rotavaporator to packed column design (Heile et al., 2014). Biogas upgrading facilities typically treat around 1/3rd of the biogas flow with 2/3rd used in combined heat and power for the production of electricity and heat, which represents an economically valuable source of heat for thermal stripping (Auty and Moore, 2003). To illustrate, in a large wastewater treatment works treating 500,000 m^3 d^{-1}, return liquors comprise 0.5% of flow (2500 m^3 d^{-1}) and biogas production is around 2500 m^3 h^{-1} (McLeod et al., 2014). Assuming 2/3rd of the biogas flow is available for heat, then the temperature gradient that can be realised in the return liquor with waste heat (kWh_{th}, 45%) is:

$$\Delta T(°C) = \frac{Available\ heat\ energy\left(\frac{kWh}{d}\right)}{S_{water}\left(\frac{kWh}{kg.°C}\right)Q_{returnliquor}\left(\frac{kg}{d}\right)} \quad (11)$$

where S_{water} is the specific heat capacity for water (0.00116 kWh kg^{-1} $°C^{-1}$). On this basis, the return liquor can be raised by a temperature difference of 50°C, which can be regarded as a conservative estimate since this does not take into consideration the inclusion of heat recovery. Importantly, this study illustrates the potential to facilitate thermal stripping with available heat, and demonstrates the recovery of extremely concentrated ammonia, where the NH_3 concentration recorded in the condensate (6.4 mol_{NH3} L^{-1}) in this study, represents the highest recorded value in the literature to the best of our knowledge, and is suitable for subsequent use in both CO_2 absorption and crystallisation.

Packed column technology has already been employed for ammonia separation from industrial wastewater at commercial scale (Zeng et al., 2006; Heile et al., 2017). However, this is usually configured as a two-stage air stripper/acid stripper (Kinidia et al., In Press), where the focus is on ammonia removal and not ammonia recovery. Ammonia concentration in the condensate recovered at 80°C was consistently 6.4 mol_{NH3} L^{-1}, independent of the rate of mass transfer, which can be ascribed to the condensate reaching the solubility limit for NH_3 for even

the lowest feed concentration such that increasing ammonia flux could not increase the condensate ammonia concentration (Figures A2 and 5; O'Neil, 2013). Reducing temperature from 80°C to 50°C almost doubles the solubility of ammonia to 12 mol_{NH3} L^{-1} (Figure A2). Therefore operating the thermal stripper at the low temperature threshold, can avoid saturation of the condensate which will markedly increase ammonia concentration, and in combination with introducing control of the reflux ratio, will help fix ammonia concentration in the recovered condensate. Mass balance on the same illustrative Wastewater Treatment Works example (McLeod et al., 2014) indicates that based on the return liquor ammonia concentration identified in this study (Table 1) and assuming 90% ammonia recovery, 367 $kmol_{NH3}$ d^{-1} are available for absorption, which closely matches the stoichiometric requirement (1:1, Equation 1) for the mass flow of CO_2 in the gas phase (333 $kmol_{CO2}$ d^{-1}). Importantly, the recovered condensate NH_3 concentration was within the range nominally proposed for CCS, illustrating its reactivity, and was above the solubility limit for NH_4HCO_3 (1.5 mol_{NH3} L^{-1}, 5°C), which evidences its viability for the initiation of direct crystallisation within the membrane contactor (Mani et al., 2006; Budzianowski, 2011b).

Carbon dioxide absorption proceeded in two-stages: an initial rapid decline in CO_2 flux up to a supersaturation ratio of around C/C* 0.5 (Figure 6), followed by a slower decline and at a lower average CO_2 flux. This can be accounted for by the initial fast reaction between CO_2 and free ammonia, followed by the reduction in pH induced by the dissolution of CO_2, which shifted the ammonia-ammonium equilibrium toward ammonium (NH_4^+). The CO_2 flux declined considerably faster for the condensate recovered from return liquor, which we propose is due to the reduction in solution surface tension (Figures 6 and 7). During thermal desorption using the rotavaporator, a small amount of liquid (and not vapour) carryover was observed at the intersection between the surface of the feed solution (round bottom flask) and condenser, which is an artefact of this lab scale device, where surface active agents partition to the air-water interface, which then passed directly into the recovered condensate. We therefore suggest the reduction in condensate surface tension is due to the concentration of surface active agents which have been shown to 'salt-out' CO_2, lowering physical solubility of CO_2 and

therefore reducing its kinetic trajectory in the second phase of absorption where physical rather chemical absorption is more dominant following the transformation from NH_3 to NH_4^+ (King, 2004). Due to the phase separation adopted in rectification, liquid carryover is less likely to occur when scaled-up. Nevertheless, the reduction in solution surface tension, which in turn reduces the breakthrough pressure of the membrane, did not evidently induce membrane wetting (Franken et al., 1987; Wang et al., 2005). This was demonstrated by the absence of gas-phase crystallisation, which is known to occur following solvent breakthrough from liquid to gas-phase (Makhloufi et al., 2014; Cui and deMontigny, 2017; Villeneuve et al., 2018).

Despite the reduction in the kinetic trajectory of absorption, the thermodynamics of crystallisation were comparable between synthetic and condensate solutions, as noted by an analogous point of induction (C/C* 1.7, Figure 7). Following dissolution, CO_2 reacts with free ammonia NH_3(aq) to produce carbamic acid (NH_2COOH); this releases hydrogen ions (H^+) which lowers pH (Wang et al., 2011). A comparable trend between pH reduction and CO_2 absorption, evidences that the reactivity of both solutions were similar (Figure 8). The carbamate (NH_2COO^-) subsequently decomposes into HCO_3^- and NH_3 but because of the pH, the ammonium-ammonia equilibrium shifts towards NH_4^+ (Kim et al., 2008; Capodaglio et al., 2015; Wang et al., 2011). Crystallisation of NH_4HCO_3 can then proceed once sufficient concentration of the reactant is present. The lag time introduced between theoretical saturation (C/C* 1) and the point of induction (C/C* 1.7) can be explained by the partial conversion of HCO_3^- into H_2CO_3 at the lower pH range, which then requires further CO_2 dissolution to achieve sufficient HCO_3^- for induction (the initiation of nucleation) (Millero and Roy, 1997). We propose that the hydrophobic membrane in this study (polypropylene, θ 117°) induced heterogeneous nucleation (Lucassen-Reynders, 1963; Curcio et al., 2006; Bougie and Iliuta, 2013):

$$\gamma_L cos\theta = \gamma_S - \gamma_{SL} \quad (12)$$

where θ is the contact angle of liquid on the membrane, while γ_L , γ_S and γ_{SL} are the surface tensions representing liquid-vapour, solid-vapour and solid-liquid interfaces, respectively. Promotion of primary heterogeneous nucleation at the membrane was confirmed by the

continued increase in crystal number observed as crystal size increased in the synthetic solution. This contradicts the behaviour of conventional crystallisers which are dominated by secondary nucleation effects that result in a decline in population density as crystal growth begins to dominate (Veiga et al., 1999). This can be explained by the membrane enabling the decoupling of nucleation from crystal growth, with nucleation continuing to proceed due to thermodynamic favourability of the membrane and the unique counter-diffusional concentration gradient that the membrane fosters between the gas and liquid phase which continues to replenish reactant at the interface (McLeod et al., 2015). Crystals were collected primarily in the downstream bulk solution, which is analogous to findings from thermally driven membrane crystallisation, and has been explained by the non-specific crystal-membrane bond formed, such that mild hydrodynamic conditions are sufficient to displace nucleated crystals form the surface (Curcio et al., 2006). The reduced surface tension of the recovered condensate served to lower the solid-liquid surface tension contribution (γ_{SL}) which implies a reduction in the activation energy required for nucleation:

$$\Delta G^* \propto \gamma_{SL}^3 \quad (13)$$

where ΔG is Gibbs free energy during critical nucleus formation. A small decrease in γ_L (and consequently γ_{SL}), will increase nucleation and growth rate which was evidenced in this study, for the recovered condensate, by the higher crystal number observed at a comparable level of supersaturation (Wu and Nancollas, 1999). We assert that induction was ostensibly the same as this was more dependent upon development of sufficient reactant to initiate induction (specifically bicarbonate). Characterisation of the solid product confirmed the crystal to be NH_4HCO_3 (Figure 11). McLeod et al. (2014) used distillation to crystallise NH_4HCO_3 in return liquors and ion-exchange regenerant following their use in biogas upgrading. However, sodium bicarbonate and calcium carbonate were respectively formed due to their thermodynamic favourability and presence in solution. In this study, pre-concentration of ammonia by thermal desorption obviated cation competition and enabled crystallisation of the preferred NH_4HCO_3 salt.

5. Conclusions

In this study, a synergy between thermal desoprtion and membrane contactor technology has been demonstrated that delivers biogas upgrading, ammonia removal from wastewater and recovery of an industrially signicant resource (crystalline ammonium bicarbonate) in a complimentary process. The following conclusions are drawn:

- Modest thermal gradients (50°C) offer more concentrative operation through suppressing water vapour pressure; higher NH_3 concentration then increases mass transfer in second stage thermal desorption. Rectification can be designed at scale to enable analogous separation within a single stage process.
- The chemistry underpinning CO_2 absorption and crystallisation in the recovered condensate was comparable to the synthetic solution. However, the condensate surface tension reduced CO_2 absorption kinetics due to 'salting-out' and enhanced the perceived nucleation rate through a reduction in the activation energy required for critical nucleus formation. We propose that the surface tension reduction identified is due to carryover of surface-active agents (e.g. surfactants) in the present study, and will not be as significant upon scale-up due to improved phase separation in thermal desorption.
- The crystalline reaction product was shown to be ammonium bicarbonate. This demonstrates that the cationic competition proviously observed in return liquors not subjected to thermal desorption, which forced the crystallisation of thermodynamically favourable salts, can be avoided by thermal pretreatment which will also inevitably improve long term maintenance of the membrane by reducing the solid and organic content of the absorbent.

Whilst the collective strength of the technologies has been demonstrated, further research is required to develop a scalable thermal stripper. This is achievable through operating the overall separation at lower temperatures to improve ammonia solubility, and mass transfer optimisation to provide stronger governance over ammonia transfer between phases.

Acknowledgements

Hermassi and McAdam were funded through European Research Council Starting Grant 714080 (SCARCE). Bavarella would like to thank Anglian Water, Northumbrian Water and Severn Trent Water for their practical and financial support. Bavarella was the recipient of a Cranfield University Industrial PhD scholarship, and benefitted from Engineering and Physical Sciences Research Council (EPSRC) support. Enquiries for access to the data referred to in this article should be directed to: researchdata@cranfield.ac.uk.

References

Al-Anezi, K., Somerfield, C., Mee, D., Hilal, N., 2008. Parameters affecting the solubility of carbon dioxide in seawater at the conditions encountered in MSF desalination plants. Desalination. 222, 548-571.

Atchariyawut, S., Jiraratananon, R., Wang, R., 2007. Separation of CO_2 from CH_4 by using gas–liquid membrane contacting process. J. Membrane Sci. 304, 163–172.

Autin, O., Hai, F., Judd, S., McAdam, E.J., 2016. Investigating the significance of coagulation kinetics on maintaining membrane permeability in an MBR following reactive coagulant dosing. J. Membrane Sci. 516, 64-73.

Auty, D., Moore, A., 2003. Digestion and Greenhouses-Synergistic Resource Recovery. 18th European Biosolids and Organic Resources Conference and Exhibition. 1, 1-12.

Bates, R., Pinching, G.D., 1949. Acidic dissociation constant of ammonium ion at 0°C to 50°C, and the base strength of ammonia. J. Res. Nat. Bur. Stand. 42, 419-430.

Bavarella, S. (2018) Chemically reactive membrane crystallisation reactor for CO_2 separation and ammonia recovery, PhD Thesis, Cranfield University, UK.

Belaissaoui, B., Favre, E., 2018. Novel dense skin hollow fiber membrane contactor based process for CO_2 removal from raw biogas using water as absorbent. Sep. Purif. Technol. 193, 112-126.

Birkmann, J., Pasel, C., Luckas, M., Bathen, D., 2018. UV spectroscopic properties of principal inorganic ionic species in natural waters. Water Practice Technol. 13, 879-892.

Bonet-Ruiz, A.E., Plesu, V., Bonet, J., Iancu, P., Llorens, J., 2015. Preliminary technical feasibility analysis of carbon dioxide absorption by ecological residual solvents rich in ammonia to be used in fertigation. Clean Technol. Envir. 17, 1313−1321.

Bougie, F., Iliuta, M.C., 2013. Analysis of Laplace–Young equation parameters and their influence on efficient CO_2 capture in membrane contactors. Sep. Purif. Technol. 118, 806-815.

Budzianowski, W.M., 2011a. Benefits of biogas upgrading to biomethane by high-pressure reactive solvent scrubbing. Biofuels Bioprod. Bioref. 6, 12-20.

Budzianowski, W.M., 2011b. Mitigating NH_3 vaporization from an aqueous ammonia process for CO_2 capture. Int. J. Chem. React. Eng. 9, 58-60.

Capodaglio, A., Hlavinek, P., Raboni, M., 2015. Physico-chemical technologies for nitrogen removal from wastewaters: a review. A&A-An Interdisciplinary Journal of Applied Science. 10, 482-493.

Chen, G., Lu, Y., Yang, X., Wang, R., Fane, A.G., 2014. Quantitative Study on Crystallization-Induced Scaling in High-Concentration Direct-Contact Membrane Distillation. Ind. Eng. Chem. Res. 53, 15656–15666.

Cui, Z., deMontigny, D., 2017. Experimental study of carbon dioxide absorption into aqueous ammonia with a hollow fiber membrane contactor. J. Membrane Sci. 540, 297–306.

Curcio, E., Fontananova, E., Di Profio, G., Drioli, E., 2006. Influence of the structural properties of poly(vinylidene fluoride) membranes on the heterogeneous nucleation rate of protein crystals. J. Phys. Chem. 110, 12438–12445.

Darde, V., Thomsen, K., Well, W.J.M., Stenby, E., 2009. Chilled ammonia process for CO_2 capture. Energy Proced. 1, 1035-1042.

Franken, A.C.M., Nolten, J.A.M., Mulder, M.H.V, Bargeman, D., Smolders, C.A., 1987. Wetting criteria for the applicability of membrane distillation. J. Membr. Sci. 33, 315–328.

He, Q., Yu, G., Tu, T., Yan, S., Zhang, Y., Zhao, S., 2017. Closing CO_2 loop in biogas production: recycling ammonia as fertilizer. Environ. Sci. Technol. 51, 8841–8850.

He, Q., Tu, T., Yan, S., Yang, X., Duke, M., Zhang, Y., Zhao, S., 2018. Relating water vapor transfer to ammonia recovery from biogas slurry by vacuum membrane distillation vacuum membrane distillation. Sep. Purif. Technol. 191, 182-191.

Heile, S., Rosenberger, S., Parker, A., Jefferson, B., McAdam, E.J., 2014. Establishing the suitability of symmetric ultrathin wall polydimethylsiloxane hollow-fibre membrane contactors for enhanced CO_2 separation during biogas upgrading. J. Membrane Sci. 452, 37–45.

Inoue, M., Hirasawa. I., The relationship between crystal morphology and XRD peak intensity on CaSO4.2H2O. J. Crystal Growth 380 (2013) 169-175.

Ji, X., Curcio, E., Obaidani, S.A., Di Profio, G., Fontananova, E., Drioli, E., 2010. Membrane distillation-crystallization of seawater reverse osmosis brines. Sep. Purif. Technol. 71, 76-82.

Kim, Y.J., You, J.K., Hong, W.H., Yi, K.B., Ko, C.H., Kim, J.N., 2008. Characteristics of CO_2 absorption into aqueous ammonia. Sep. Sci. Technol. 43, 766-777.

King, A.D., 2004. The solubility of ethane, propane, and carbon dioxide in aqueous solutions of sodium cumene sulfonate, J. Colloid Interface Sci. 273, 313-319.

Kinidia, L., Tan, I.A.W., Wahab, N. B. A., Tamrin, K. F. B., Hipolito, C. N., Salleh, S.F., Recent development in ammonia stripping process for industrial wastewater treatment, International Journal of Chemical Engineering, Article ID 3181087, 14 pages https://doi.org/10.1155/2018/3181087

Kozak, F., Petig, A., Morris, E., Rhudy, R., Thimsen, D., 2009. Chilled ammonia process for CO_2 capture. Energy Proced. 1, 1419-1426.

Li, K., Kong, J., Tan, X., 2000. Design of hollow fibre membrane modules for soluble gas removal. Chem. Eng. Sci. 55, 5579–5588.

Lucassen-Reynders, E.H., 1963. Contact angles and adsorption on solids. J. Phys. Chem. 67, 969-972.

Ma, X., Li, Y., C., H., Duan, F., Su, C., Lu, C., Chang, J., Ding, H., 2019. High-selectivity membrane absorption process for recovery of ammonia with electrospun hollow fiber membrane, Sep. Purif. Technol. 216, 136-146.

Makhloufi, C., Lasseuguette, E., Remigy, J.C., Belaissaoui, B., Roizard, D., Favre, E., 2014. Ammonia based CO_2 capture process using hollow fiber membrane contactors. J. Membrane Sci. 455, 236–246.

McLeod, A., Buzatu, P., Autin, O., Jefferson, B., McAdam, E., 2015. Controlling shell-side crystal nucleation in a gas–liquid membrane contactor for simultaneous ammonium bicarbonate recovery and biogas upgrading. J. Membrane Sci. 473, 146–156.

McLeod, A., Jefferson, B., McAdam, E., 2014. Biogas upgrading by chemical absorption using ammonia rich absorbents derived from wastewater. Water Res. 67, 175-186.

Meng, L., Burris, S., Bui, H., Pan, W.P., 2005. Development of an Analytical Method for Distinguishing Ammonium Bicarbonate from the Products of an Aqueous Ammonia CO_2 Scrubber. Anal. Chem. 77, 5947-5952.

Millero, F., Roy, R.N., 1997. A Chemical Equilibrium Model for the Carbonate System in Natural Waters. Croat. Chem. Acta. 70, 1-38.

Mookherji, A., Tandon, S.P., 1966. Influence of concentration on the ultraviolet absorption spectrum of bicarbonate ion in state of aqueous solution, J. Phys. Soc. Japan 21, 1176- 1178.

Mortson, M., Telesz, R.W., 2001. Flue gas desulphurisation using recycled sodium bicarbonate, USEPA/DOE/EPRI Combined power plant air pollutant control symposium: the mega symposium, August 20-23, Chicago, US.

O'Neil, M.J., 2013. The Merck Index - An Encyclopedia of Chemicals, Drugs, and Biologicals. 1, 88-100.

Oxera Consulting Ltd, 2006. What is the cost of reducing ammonia, nitrates and BOD in sewage treatment works effluent? Report prepared for Ofwat. (Accessed 13th March, 2018).

Perry, R.H., Green, D.W., 2007. Perry's Chemical Engineers' Handbook. 8, 2-126.

Persson, M., Jonsson, O., Wellinger, A., 2007. Task 37-Biogas Upgrading to Vehicle Fuel Standards and Grid Injection. IEA Bioenergy. 1, 8-9.

PubChem, 2004. U.S. National Library of Medicine. Retrieved from https://pubchem.ncbi.nlm.nih.gov/compound/ammonium_bicarbonate (Accessed 21th June, 2018).

Salavera, D., Chaudhari, S.K., Esteve, X., Coronas, A., 2005. Vapor-liquid equilibria of ammonia + water + potassium hydroxide and ammonia + water + sodium hydroxide solutions at temperatures from 293.15 to 353.15K. J. Chem. Eng. Data. 50, 471-476.

Shuangchen, M., Huihui, S., Bin, Z., Gongda, C., 2013. Experimental study on additives inhibiting ammonia escape in carbon capture process using ammonia method. Chem. Eng. Res. Des. 91, 2775-2781.

Sutter, D., Gazzani, M., Mazzotti, M., 2015. Formation of solids in ammonia-based CO_2 capture processes — Identification of criticalities through thermodynamic analysis of the CO_2–NH_3–H_2O system. Chem. Eng. Sci. 133, 170-180.

Tao, W., Ukwuani, A.T., 2015. Coupling thermal stripping and acid absorption for ammonia recovery from dairy manure: ammonia volatilization kinetics and effects of temperature, pH and dissolved solids content. Chem. Eng. J. 280, 188-196.

Teichgraber, B., Stein, A., 1994. Nitrogen elimination from sludge treatment reject water-comparison of the steam-stripping and denitrification processes. Wat. Sci. Technol. 30, 41-51.

Thurston, R.V., Russo, R.C., Emerson, K., 1979. Aqueous Ammonia Equilibrium – Tabulation of Percent Un-ionised Ammonia, United States Environmental Protection Agency, (EPA-600 3-091). 1, 1-427.

Ukwuani, A.T., Tao, W., 2016. Developing a vacuum thermal stripping-acid absorption process for ammonia recovery from anaerobic digester effluent. Water Res. 106, 108-115.

Vecino, X., Reig, M., Bhushan, B., Gibert, O., Valderrama, C., Cortina, J.L., 2019. Liquid fertilizer production by ammonia recovery from treated ammonia-rich regenerated streams using liquid-liquid membrane contactors. Chem. Eng. J. 360, 890-899.

Veiga, A.R., Calmanovici, C.E., Giulietti, M., 1999. Operational conditions evaluation in ammonium bicarbonate crystallisation. Proceedings of the 14th International Symposium on Industrial Crystallization. 65, 1−12.

Villeneuve, K., Roizard, D., Remigy, J.C., Iacono, M., Rode, S., 2018. CO_2 capture by aqueous ammonia with hollow fiber membrane contactors: Gas phase reactions and performance stability. Sep. Purif. Technol. 199, 189-197.

Wang, R., Zhang, H.Y., Feron, P.H.M., Liang, D.T., 2005. Influence of membrane wetting on CO_2 capture in microporous hollow fiber membrane contactors, Sep. Purif. Technol. 46, 33–40.

Wang, X., Conway, W., Fernandes, D., Lawrance, G., Burns, R., Puxty, G., Maeder, M., 2011. Kinetics of the reversible reaction of CO_2(aq) with ammonia in aqueous solution. J. Phys. Chem. 115, 6405-6412.

Whitfield, M., 1974. The hydrolysis of ammonium ions in sea water - a theoretical study. Mar. Biol. Assoc. 54, 565-580.

Wilson, N.S., Morrison, R., Dolan, J.W., 2001. Buffers and Baselines. LC-GC Europe. 1, 1-3.

Wilson, T., 1925. The total and partial vapor pressures of aqueous ammonia solutions. University of Illinois bulletin. 22, 1-50.

Wu, W., Nancollas, G.H., 1999. Determination of interfacial tension from crystallization and dissolution data: a comparison with other methods. Adv. Colloid Interfac. 79, 229-279.

Yeh, J.T., Resnik, K.P., Rygle, K., Pennline, H.W., 2005. Semi-batch absorption and regeneration studies for CO_2 capture by aqueous ammonia. Fuel Process. Technol. 86, 1533-1546.

Zeng, L., Mangan, C., Li, X., 2006. Ammonia recovery from anaerobically digested cattle manure by steam stripping. Water Sci. Technol. 54, 137-145.

(a)

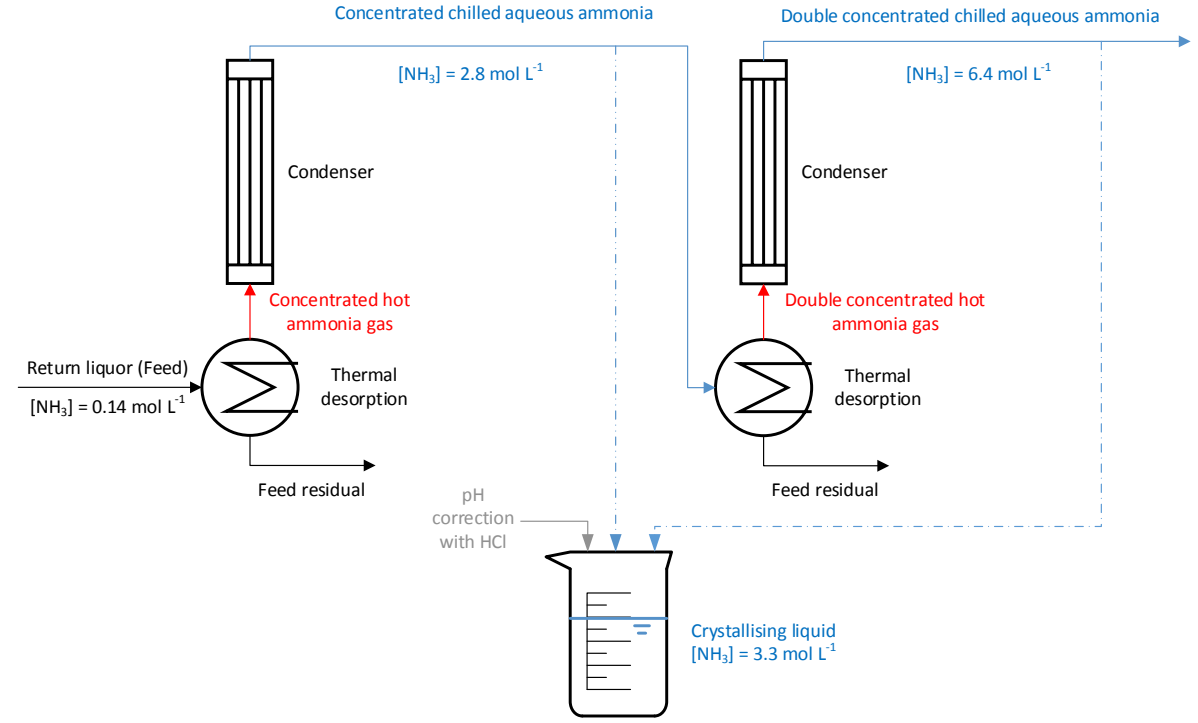
Concentrated chilled aqueous ammonia
[NH3] = 2.8 mol L-1
Double concentrated chilled aqueous ammonia
[NH3] = 6.4 mol L-1
Condenser
Condenser
Concentrated hot ammonia gas
Double concentrated hot ammonia gas
Return liquor (Feed)
[NH3] = 0.14 mol L-1
Thermal desorption
Thermal desorption
Feed residual
Feed residual
pH correction with HCl
Crystallising liquid
[NH3] = 3.3 mol L-1

(b)

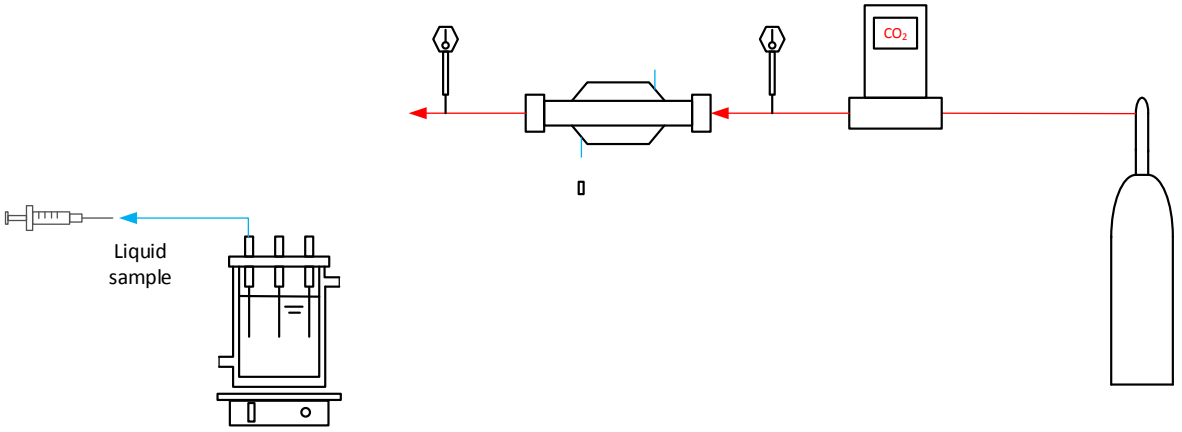
Temperature sensor
CO2
Liquid sample

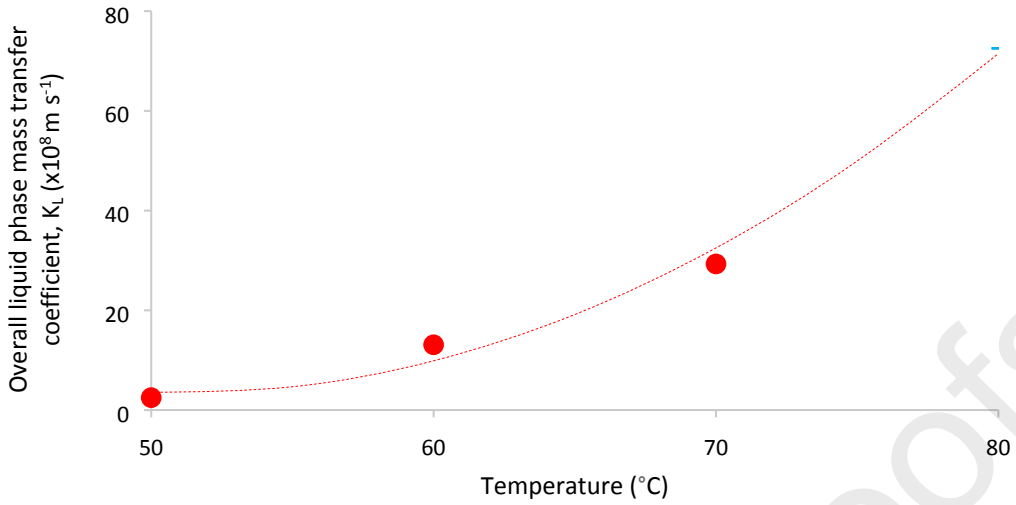

Figure 2. Impact of temperature on the rate of primary stage ammonia desorption, where feed solution concentration is equivalent to return liquor (1.8 g L^{-1}, 0.11 mol L^{-1}). Operating conditions: vacuum, 100 mbar; pH = 11; $V_{recovered}/V_{feed(initial)}$, 2%.

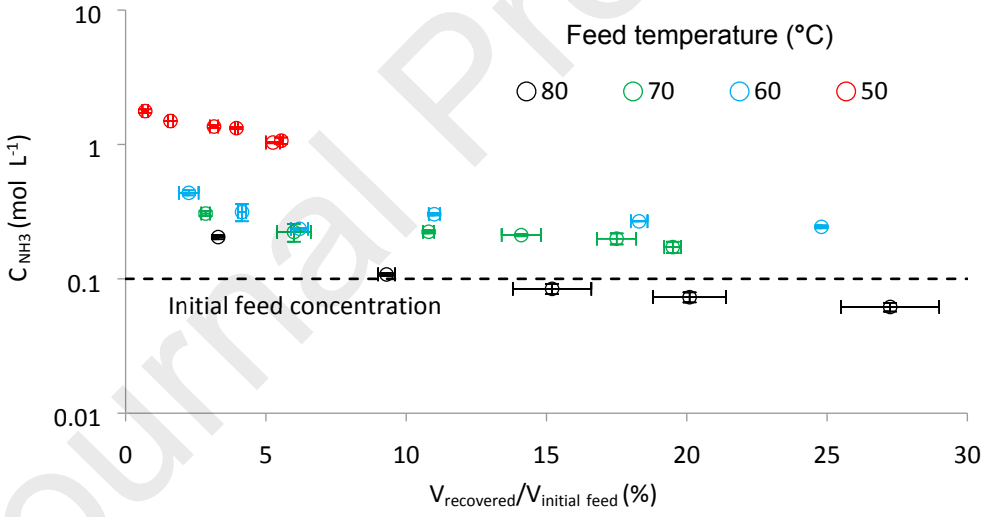

Figure 3. Impact of temperature on the recovered condensate ammonia concentration (C_{NH3}), where feed soluton concentration is equivalent to return liquor (1.8 g L^{-1}, 0.11 mol L^{-1}). Operating conditions: vacuum, 100mbar; initial volume, 1000 mL; pH = 11. Error bars indicate standard deviation from sacrificial experiments undertaken in triplicate.

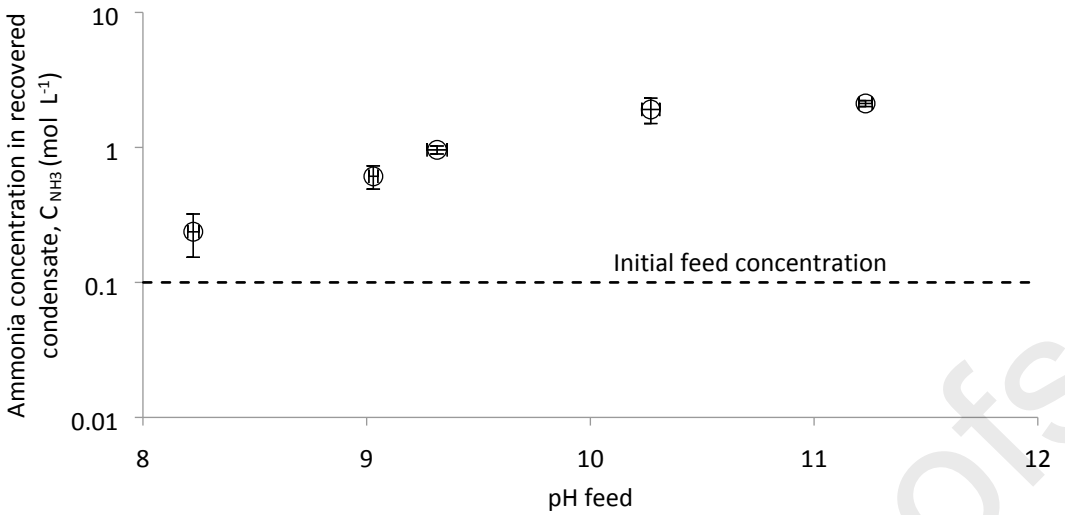

Figure 4. Impact of pH on the recovered condensate ammonia concentration (C_{NH3}), where feed soluton concentration is equivalent to return liquor (1.8 g L^{-1}, 0.11 mol L^{-1}). Operating conditions: vacuum, 420 mbar; desorption time, 45 mins.; temp., 80 °C. Error bars indicate standard deviation from sacrificial experiments conducted in triplicate.

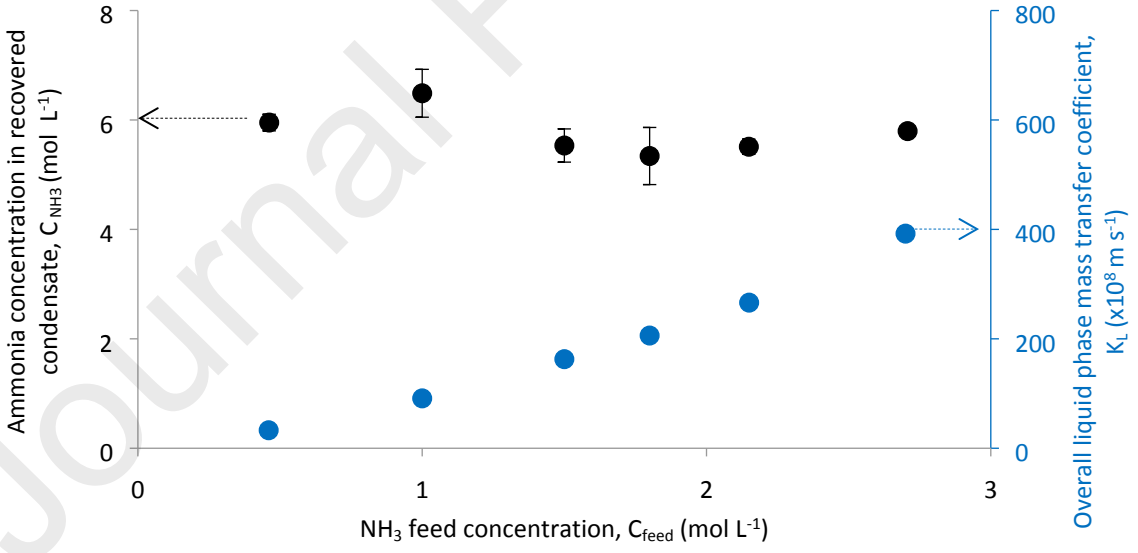

Figure 5. Impact of NH_3 feed concentration on second stage thermal desorption characterising mass transfer and the condensate NH_3 concentration achieved. Operating conditions: vacuum, 470mbar; desorption time, 45 mins.; temp., 80°C; initial vol., 1000mL; pH = 12. Error bars indicate standard deviation.

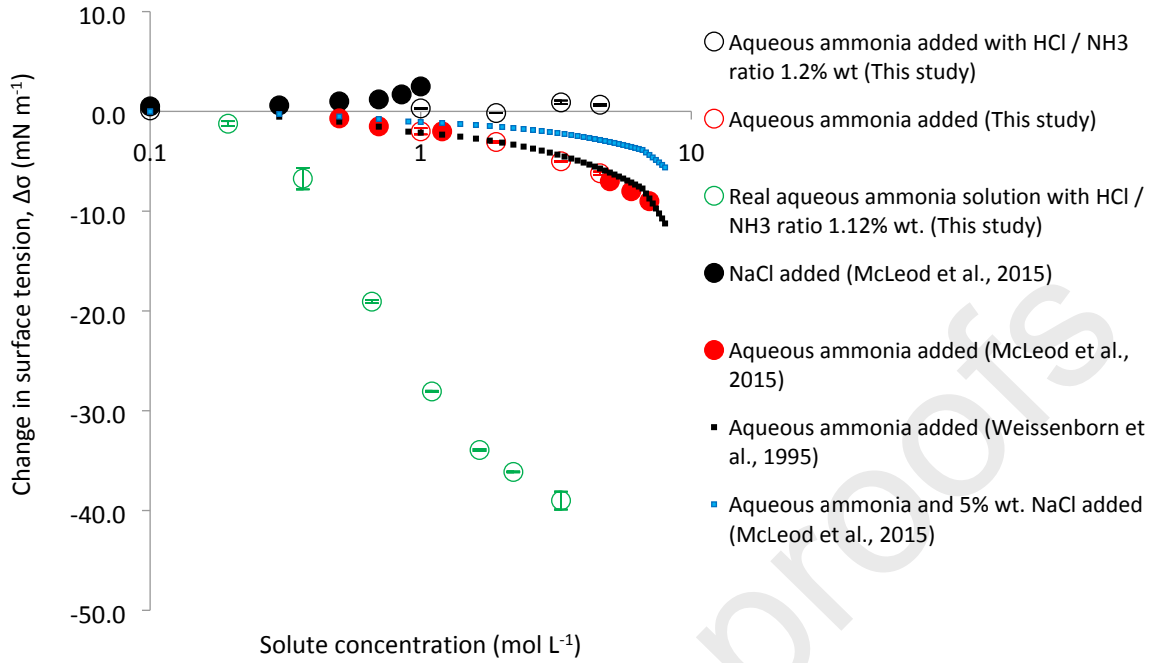

Figure 6. Comparison of surface tension determined for the recovered condensate, synthetic solution and relevant literature sources.

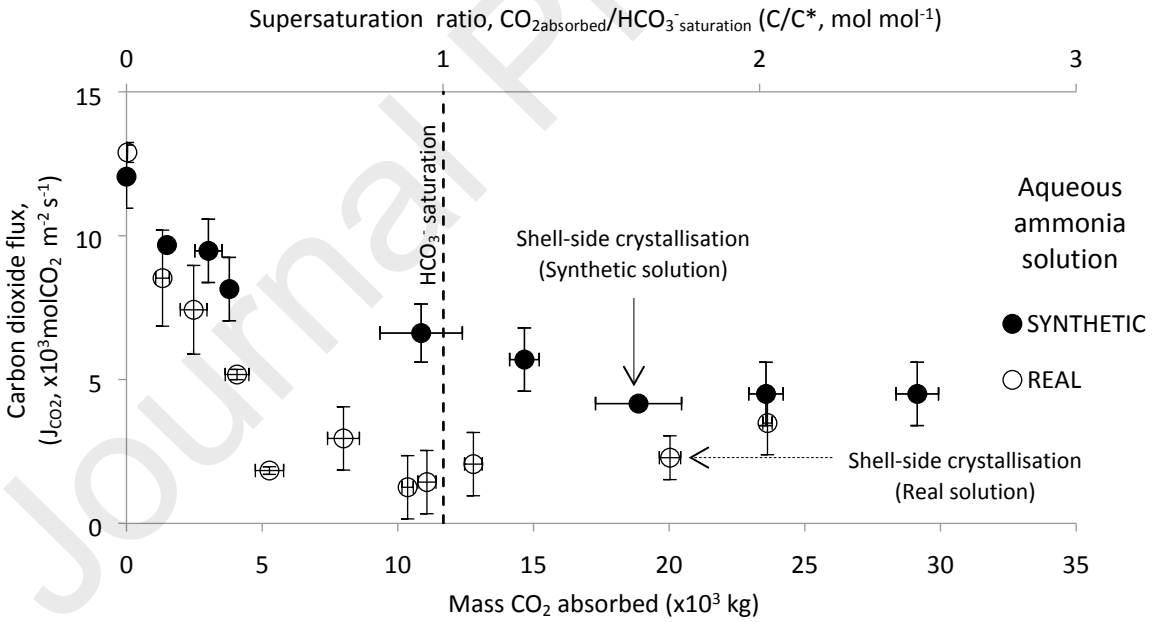

Figure 7. Carbon dioxide flux through the membrane during absorption using synthetic and real ammonia (3.3M). Operation conditions: liquid shell-side; Liquid temp., 5°C; G/L, 5; V_L, 0.06 m s^{-1}; V_G, 14.7 m s^{-1}. Shell-side crystallisation occurred at C/C*≈1.7 for both solutions. Error bars indicate standard deviation from sacrificial experiments undertaken in triplicate.

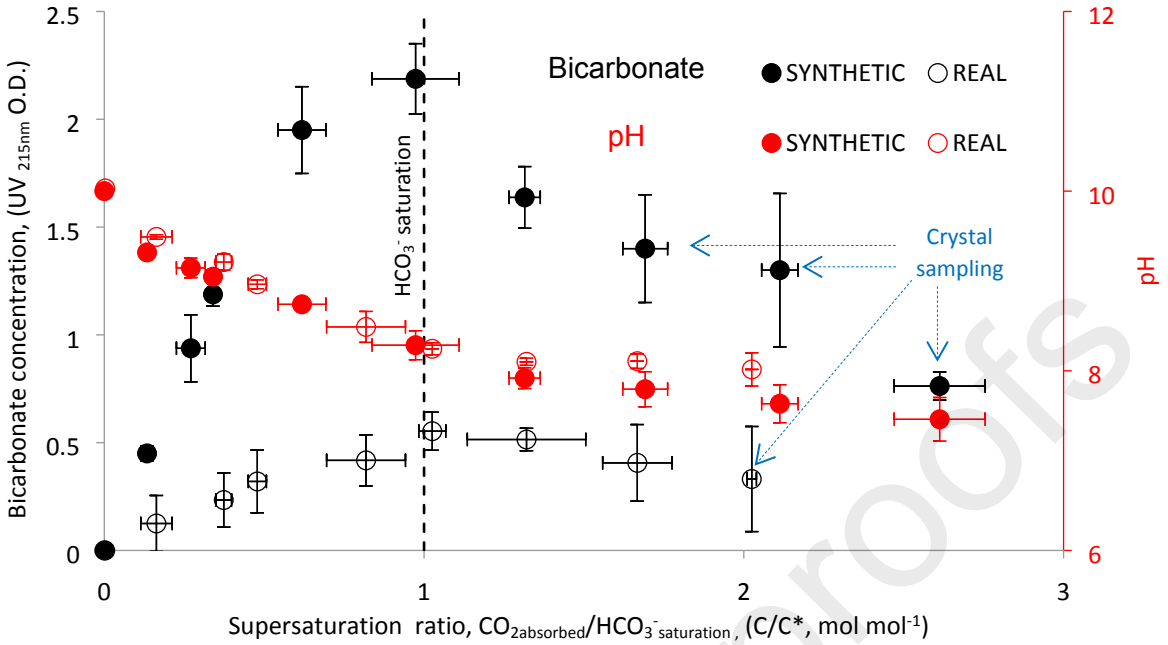

Figure 8. Impact of progressive CO_2 absorption on pH and bicarbonate formation (determined at UV_{215nm}). Operating conditions: liquid shell-side; Liquid temp., 5°C; NH_3 3.3M; G/L, 5; V_L, 0.06 m s^{-1}; V_G, 14.7 m s^{-1}. Error bars indicate standard deviation from sacrificial experiments undertaken in triplicate.

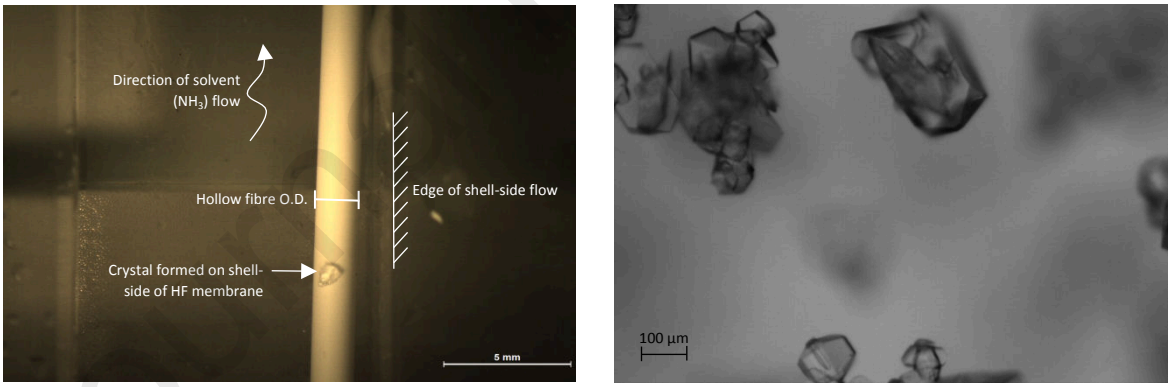

(a) (b)

Figure 9. Ammonium bicarbonate crystal formation observed in real time (C/C* ~1.5-1.8): (a) on the membrane during CO_2 absorption through the direct observation cell window (top-side view); and (b) in the bulk solution downstream of the membrane using in-situ particle visual microscopy (PVM).

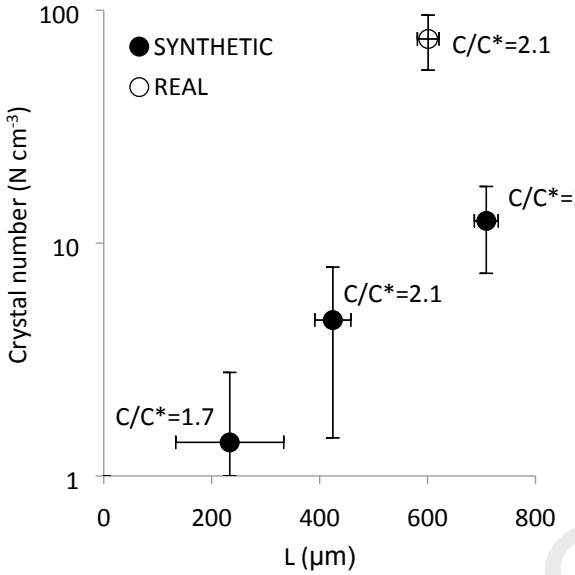

Figure 10. Comparison of crystalline ammonium bicarbonate formation by the membrane using synthetic and recovered condensate solutions of equivalent ammonia concentration (3.3 mol L^{-1}; 46.2 gN-NH_3 L^{-1}). Operating conditions: G/L, 5; V_L, 0.06 m s^{-1}; V_G, 14.7 m s^{-1}; Liquid temp., 6±1°C; Gas temp., 19±1°C Error bars indicate standard deviation from sacrificial experiments undertaken in triplicate.

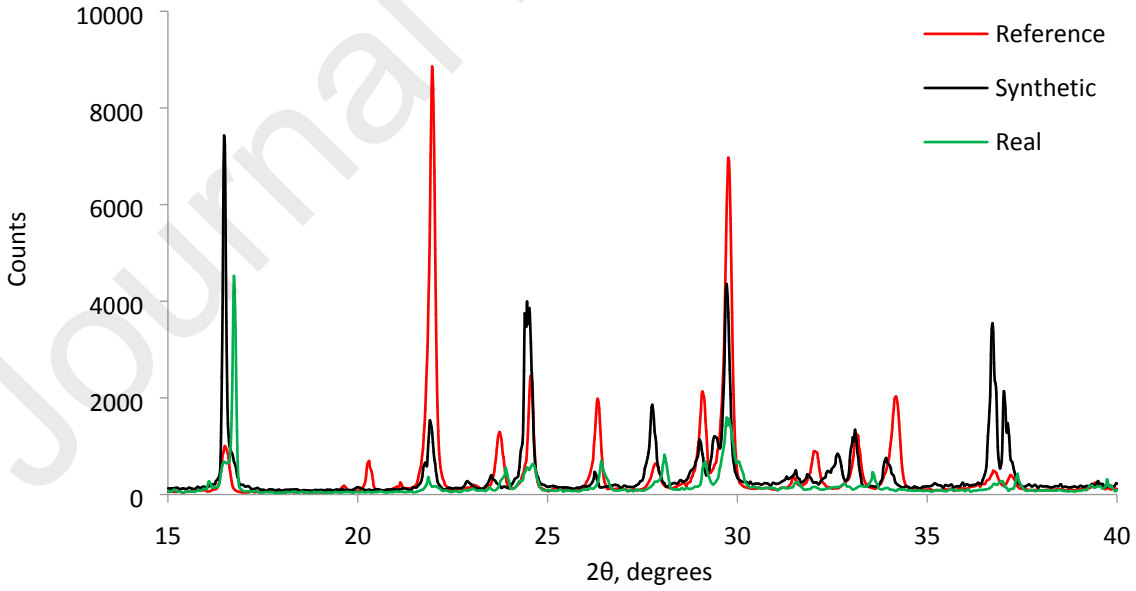

Figure 11. XRD analysis of pure NH_4HCO_3 (Reference), crystalline ammonium bicarbonate produced from recovered condensate using the membrane (return liquor; real), and ammonium bicarbonate crystallised from synthetic solution using the membrane (Synthetic).

Table 1. Characterisation of return liquor and condensate from first and second stage of NH_3(aq) recovery process.

		Return Liquor	Condensate		Crystallising fluid [a]	Synthetic fluid
			First Stage	Second Stage		
pH	(-)	8.4	11.5	11.5	11.3	12.6
COD[a]	mg L^{-1}	6100	486	1767	913	<25
SCOD[b]	mg L^{-1}	4500	427	1678	844	<25
TSS[c]	mg L^{-1}	6600	LD	LD	LD	LD
Conductivity	mS cm^{-1}	2.05	1.59	0.87	1.35	0.19
$[NH_3]_{initial\ feed}$	mol_{NH3} L^{-1}	0.14	2.8	6.4	3.3[d,e]	3.3[e]
	gNH_3-N L^{-1}	2.0	39.2	89.6	56	56

[a] Chemical oxygen demand. [b] Soluble chemical oxygen demand. [c] Total suspended solids. [d] Mixture between first and second stage condensates to fix NH_3 at 4M before pH correction. [e] Initial 4M concentration lowered to 3.3M NH_3 following pH correction with HCl to pH10. LD – Limit of detection.

Table 2. Operation of two-stage thermal desorption of ammonia from return liquor.

		Stage	
		First	Second
Feed temperature	°C	80	80
Vacuum pressure	mbar	420	470
Desorption time	min	60	45
Volume initial feed	mL	1000	1000
pH initial feed	(-)	11[a]	11.5
$[NH_3\text{-}N]_{initial\ feed}$	mol_{NH3} L^{-1}	0.14	2.8
	gNH_3-N L^{-1}	2.0	39.2
$[NH_3\text{-}N]_{condensate}$	mol_{NH3} L^{-1}	2.8	6.4
	gNH_3-N L^{-1}	39.2	89.6

[a]Addition of 1% sodium hydroxide to ensure equilibrium is shifted 100% toward ammonia (NH_3).

Appendices

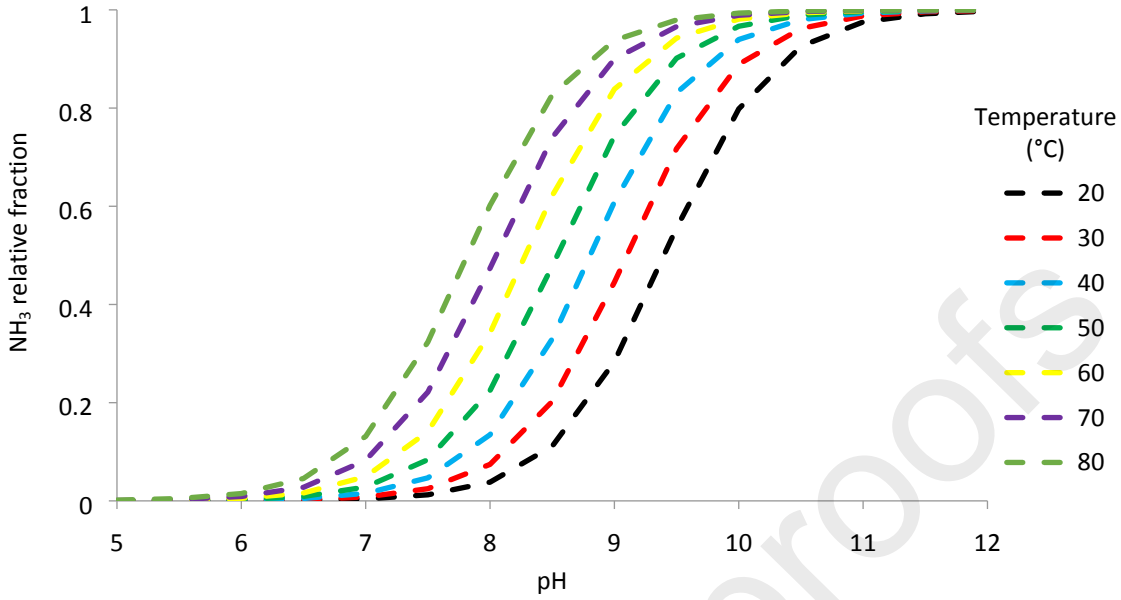

Figure A1. Impact of liquid temperature and pH on ammonia-ammonium equilibrium (Bates and Pinching, 1949).

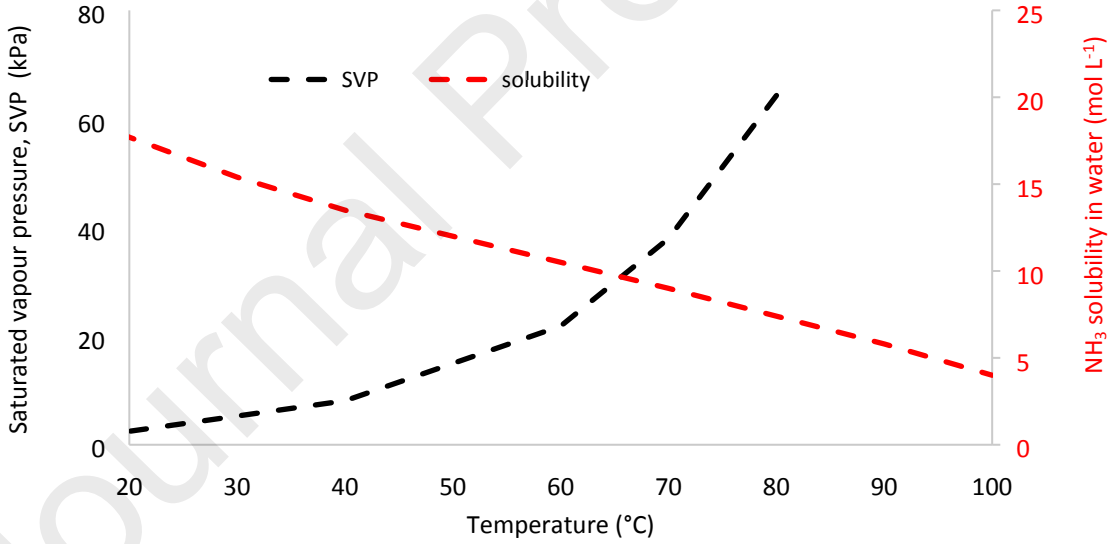

Figure A2. Saturated vapour pressure of NH_3(aq) at 1.8gNH_3-N L^{-1} (black line), and ammonia solubility in water (red line) with change in solution temperature (O'Neil, 2013).

(a) (b) (c)

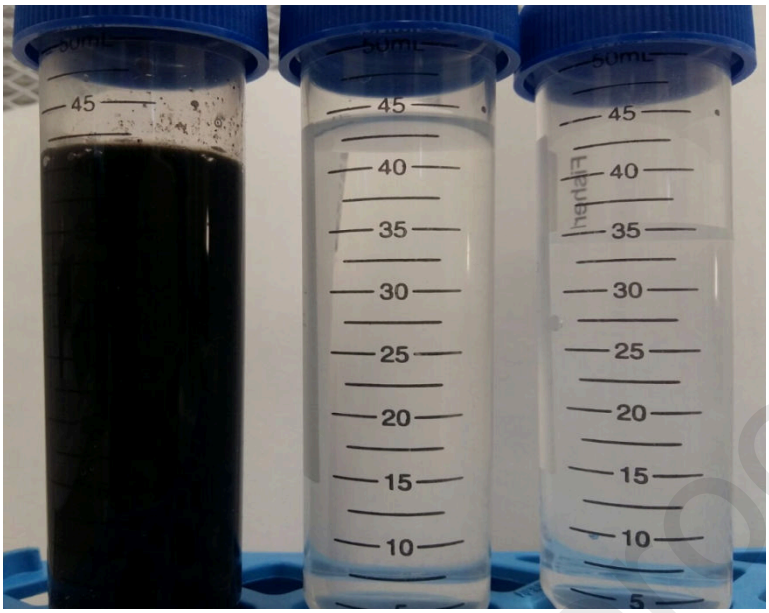

Figure A3. Images of: (a) return liquor used in this study; (b) condensate produced for membrane chemically assisted crystallisation; and (c) ultra-pure water.

Table A1. Dimensions and surface characteristics of the single membrane fibre.

Fibre characteristics		
Membrane material	-	polypropylene
Inner diameter	mm	1.2
Outer diameter	mm	1.8
Wall thickness	µm	300
Active length	mm	165
Surface area[b]	m^2	9.33×10^{-4}
Nominal pore size[a]	µm	0.2
Lumen cross sectional area	m^2	1.13×10^{-6}
Shell side characteristics		
Height	mm	5
Width	mm	12
Shell cross sectional area	m^2	6.0×10^{-5}
Priming volume	ml	11.0
Operational characteristics		
Flow regime		Counter-current
Shell-side		3.3 M NH_3 (aq)
Lumen-side		99.8% CO_2
Liquid temperature	°C	6 ± 1
Gas temperature	°C	19 ± 1

[a] Data provided by manufacturer. [b] Based on fibre outer diameter.

Highlights

- Thermal desorption concentrates ammonia from return liquor up to 109,000 mg L^{-1}
- Concentrated is effectively demonstrated for separation CO_2 from biogas
- Membrane lowers activation energy barrier to induce crystallisation
- Absorption rate for ammonia concentrate and synthetic same but nucleation increases
- Crystals confirmed to be ammonium bicarbonate proving minimal cationic competition

Credit Author Statement

S. Bavarella	Conceptualisation, Data Curation, Investigation, Methodology, Writing – original draft
M. Hermassi	Data curation, Investigation, Methodology, Writing - review
A. Brookes	Conceptualisation, Funding acquisition, Writing - review
A. Moore	Conceptualisation, Funding acquisition, Writing - review
P. Vale	Conceptualisation, Funding acquisition, Writing - review
I.S. Moon	Formal analysis, Writing - editing
M. Pidou	Funding acquisition, Supervision, Writing - editing
E.J. McAdam	Conceptualisation, Funding acquisition, Supervision, Writing - editing

Recovery and concentration of ammonia from return liquor to promote enhanced CO2 absorption and simultaneous ammonium bicarbonate crystallisation during biogas upgrading in a hollow fibre membrane contactor

Bavarella, Salvatore

2020-01-27

Bavarella S, Hermassi M, Brookes A, et al., (2020) Recovery and concentration of ammonia from return liquor to promote enhanced CO2 absorption and simultaneous ammonium bicarbonate crystallisation during biogas upgrading in a hollow fibre membrane contactor. Separation and Purification Technology, Volume 241, June 2020, Article number 116631

https://doi.org/10.1016/j.seppur.2020.116631